EAI Endorsed Transactions
on Energy Web

Research Article EAI.EU

Refined 3D Gaussian Splatting Method for Distribution Network Modeling Towards AR-Oriented Operation and Maintenance

Conghan Liu[1*], Lijuan Yan[2], Linjun Lu[1], Huazhang Tan[3]

[1]Electric Power Research Institute of Guangxi Power Grid Co., Ltd, Nanning 530023, China
[2]Guangxi Power Grid Co., Ltd, Nanning 530023, China
[3]Liuzhou Power Supply Bureau of Guangxi Power Grid Co., Ltd, Liuzhou 545000, China

Abstract

Aiming at the problems of missing slender structure modeling, complex background interference, and algorithm efficiency bottlenecks in the 3D reconstruction of distribution networks, this paper proposes an improved 3D Gaussian splatting-based algorithm for 3D reconstruction of distribution network scenes. First, through a semantics-guided density control strategy combined with adversarial background suppression, power equipment and vegetation artifacts are effectively separated. Second, a direction-sensitive covariance optimization method is designed to enhance the geometric continuity and detail fidelity of ultra-slender structures such as power lines and utility poles. Finally, a lightweight progressive splatting framework is constructed to achieve real-time rendering at ≥35 fps under 1080p resolution. Experiments show that the improved algorithm significantly increases the completeness rates of power lines, utility poles, and insulators to 90%, 95%, and 80%, respectively, reduces background artifacts to 2% in area, and shortens the reconstruction time to 0.4 hours. This study provides a high-precision modeling tool for digital twins of distribution networks and supports real-time applications of augmented reality (AR) technology in inspection navigation, fault localization, and remote collaboration.

Keywords: Distribution Network; 3D Reconstruction; Digitization; 3D Gaussian Splatting; Augmented Reality (AR)

Received on 19 November 2025, accepted on 14 December 2025, published on 31 March 2026

doi: 10.4108/ew.11921

1. Introduction

With the advancement of energy transition and the "Dual Carbon" goals, the digitalization of distribution networks has become one of the core tasks in building a new-type power system [1,2]. As a key technological support for distribution network digitalization, high-precision 3D reconstruction can provide geometric, topological, and environmental information of the physical grid for digital twin platforms [3,4], serving as the foundation for equipment condition monitoring, fault simulation, and intelligent maintenance [5,6]. Particularly for augmented reality (AR)-driven field operations (such as inspection navigation and remote collaboration), centimeter-level accuracy and real-time rendering capabilities are core prerequisites for ensuring precise alignment between virtual information and physical equipment. In recent years, domestic and international studies have emphasized that the refined modeling of critical equipment (e.g., utility poles, power lines, and insulators) and the reconstruction of complex surrounding scenes (e.g., vegetation and buildings) in distribution networks are crucial for improving grid simulation accuracy and operational efficiency [7,8]. For instance, sag calculation of power lines requires millimeter-level precision to avoid discharge risks, while defect detection on insulator surfaces relies on high-resolution textural information [9,10,11]. However, existing

*Corresponding author. Email: 514494241@qq.com

3D reconstruction technologies still face significant challenges in complex power scenarios.

Traditional methods such as LiDAR-based point cloud reconstruction can capture the geometric information of power equipment, but they often suffer from model discontinuities in slender structures like power lines due to point cloud sparsity [12,13]. While emerging Neural Radiance Field (NeRF) techniques have shown excellent performance in natural scenes [14], their reliance on dense viewpoint inputs and high computational resources makes them unsuitable for field environments with low-texture power lines and complex backgrounds (e.g., vegetation occlusion). These methods frequently exhibit issues such as missing power lines, blurred backgrounds, and loss of details [15]. Moreover, existing algorithms face a bottleneck in balancing efficiency and quality: high-precision models often require super-linear computational costs, making it difficult to meet the demands of real-time simulation in distribution networks [16,17]. Therefore, there is an urgent need for a 3D reconstruction method that simultaneously addresses precision, efficiency, and scene adaptability to support the transition of distribution network digital twins from "visualization" to "computability."

The limitations of current 3D reconstruction technologies for distribution networks can be summarized into three aspects:

(1) Deficiencies in modeling slender structures and low-texture features: Targets such as power lines exhibit small diameters (typically <5 cm) and uniform surface textures, causing methods based on photogrammetry or neural rendering to fail in complete reconstruction due to feature matching failures [18].

(2) Accuracy degradation under complex background interference: Distribution networks are often located in vegetation-dense or building-intensive areas. Traditional point cloud segmentation algorithms struggle to distinguish power equipment from background objects, while NeRF-based methods tend to generate blurred artifacts in occluded scenes [19].

(3) Trade-off between algorithmic efficiency and reconstruction quality: Existing high-precision methods, such as multi-scale NeRF, require training times ranging from hours to days, failing to meet the timeliness demands of dynamic simulation and rapid updates in distribution networks [20].

These issues severely constrain the application of digital twin technology in distribution network planning, inspection, and disaster warning. For example, discontinuities in power line models may lead to errors in sag calculation, while background blurring can interfere with the reliability of autonomous obstacle avoidance algorithms for drones.

To address the aforementioned challenges, this paper proposes an improved 3D Gaussian Splatting algorithm tailored for distribution network scenarios. Its core innovations include:

(1) Hierarchical Background Separation and Detail Preservation: A semantics-guided Gaussian density control strategy is designed, combined with adaptive occlusion culling, to reconstruct geometric features of utility poles while suppressing vegetation artifacts.

(2) Anisotropic Covariance-Based Optimization for Power Line Modeling: By introducing direction-sensitive Gaussian kernel functions and an intensity-edge feature fusion mechanism, the spatial continuity and noise resistance of slender structures are enhanced.

(3) Lightweight Parallel Splatting Framework: The GPU-accelerated sorting and blending pipeline is optimized through sparse projection and progressive gradient propagation, achieving real-time rendering (≥30 fps) at 1080p resolution while ensuring sub-centimeter accuracy.

This study aims to resolve the coupled challenges of missing slender structures, background interference, and efficiency bottlenecks in 3D reconstruction of distribution networks, providing a new generation of modeling tools for digital twins that balance precision and practicality.

2. 3D Gaussian Splatting Algorithm

2.1 Principle and Characteristics Analysis of 3D Gaussian Splatting Algorithm

3D Gaussian Splatting is a scene representation and rendering technique based on explicit Gaussian primitives. Its core objective is to achieve real-time rendering while ensuring high-precision reconstruction by dynamically optimizing the geometric and optical properties of anisotropic Gaussian primitives. This algorithm combines the controllability of explicit geometric representation with the continuity advantages of implicit volume rendering, demonstrating significant potential in natural scene reconstruction in recent years. Its technical framework can be decomposed into the following three core modules:

(1) Gaussian Parameterization and Dynamic Optimization: Collaborative Modeling of Geometry and Optics

The algorithm uses a set of optimizable Gaussian primitives as the basic units of the scene. Each Gaussian primitive includes geometric properties (center position, covariance matrix, opacity) and optical properties (spherical harmonic coefficients encoding color).

The covariance matrix is decomposed into a rotation matrix R and a scaling matrix S through the following factorization:

$$\Sigma = RSS^T R^T \tag{1}$$

This approach effectively avoids the risks associated with directly optimizing non-positive semi-definite matrices while enabling flexible control over anisotropy. For instance, primitives can be elongated into ellipsoids to align with the trajectory of power lines or flattened into disc-like shapes to characterize insulator surfaces.

During optimization, the algorithm jointly adjusts all parameters via stochastic gradient descent (SGD), combined with an adaptive density control strategy—cloning, splitting, and pruning Gaussians—to dynamically refine the distribution of primitives. In low-texture regions, cloning increases primitive density to compensate for feature gaps, while in background areas, splitting refines primitives to suppress artifacts. This dynamic optimization mechanism allows the algorithm to progressively converge from a sparse initial point cloud to a high-precision model while maintaining memory efficiency.

(2) Differentiable Splatting Rendering Mechanism

During the rendering stage, the algorithm projects 3D Gaussians onto 2D screen space, achieving efficient imaging through tile-based sorting and blending. In this process, the screen is divided into 16×16 pixel tiles, retaining only Gaussians intersecting with the view frustum and leveraging GPU-parallelized radix sort for depth-based ordering. Subsequently, pixel colors are computed using the standard alpha-blending formula:

$$C = \sum_{i=1}^{N} T_i \alpha_i c_i \tag{2}$$

where:

$$T_i = \prod_{j=1}^{i-1} (1 - \alpha_j) \tag{3}$$

This approach not only enables real-time rendering (≥25 fps) but also facilitates differentiable optimization of Gaussian primitive parameters by recording cumulative transparency along the blending path T_i. Compared to traditional NeRF's stochastic sampling, splatting rendering eliminates the computational overhead of ray integration while resolving ordering ambiguities in overlapping transparent objects through visibility-based sorting.

(3) Strategy for Balancing Efficiency and Quality

To balance computational efficiency and reconstruction quality, the algorithm employs a hierarchical optimization framework. In the early training stages, low-resolution images are used to quickly capture the main scene structure, with resolution gradually increased to refine details. During the rendering phase, resource consumption is reduced through sparse projection (processing only visible Gaussians) and dynamic memory scheduling.

2.2 Advantages and Limitations of 3D Gaussian Algorithm

Advantages

(1) Efficiency of Explicit Geometric Representation

Unlike implicit neural radiance fields (NeRF) that rely on MLP inference and stochastic sampling, 3D Gaussian primitives as explicit geometric elements can be directly processed through the GPU rasterization pipeline, avoiding the computational overhead of per-ray integration. Experiments demonstrate that it achieves real-time rendering at ≥25 fps under 1080p resolution, with training speeds 10-100 times faster than NeRF (e.g., Mip-NeRF360 requires 48 hours, while 3D Gaussian Splatting only needs 30-45 minutes).

(2) Flexibility of Anisotropic Modeling

By optimizing the covariance matrix, Gaussian primitives can adaptively stretch into ellipsoids with an aspect ratio of up to 5:1, effectively capturing geometric features of slender structures such as cross-arms of utility poles and wire connectors. Compared to traditional point clouds (prone to fragmentation) or isotropic voxels (lacking detail), anisotropic modeling offers significant advantages in reconstructing local geometry of power equipment.

(3) Robustness of Dynamic Density Control

The adaptive addition and pruning strategy enables the algorithm to progressively refine from sparse inputs (e.g., only SfM point clouds) to millions of Gaussian primitives while maintaining model compactness in complex scenes. For example, optimizing insulator strings can precisely characterize individual disc-shaped structures by splitting primitives without relying on high-density point cloud inputs.

(4) Detail Preservation and Noise Resistance

The smooth attenuation characteristics (exponential function) of Gaussian primitives effectively mitigates common issues in point cloud reconstruction, such as holes and jagged edges, particularly generating continuous surfaces even in low-texture regions. Additionally, the ability of spherical harmonic coefficients to model viewpoint-dependent lighting can restore local reflectivity variations caused by contamination on insulators.

Limitations

While 3D Gaussian algorithms demonstrate excellent performance in general scenarios, they still face the following critical bottlenecks in the specialized application context of distribution networks:

(1) Insufficient Modeling Precision for Ultra-Slender Structures

The diameter of targets such as power lines is typically less than 5 cm. Existing covariance optimization methods lack sufficient sensitivity to primitives with aspect ratios >10:1, often leading to model discontinuities due to numerical instability (e.g., gradient vanishing or covariance matrix degeneration). Experiments indicate that reconstruction errors at power line crossing points can reach 10-20 cm, far exceeding safety thresholds.

(2) Artifact Issues Under Complex Background Interference

In vegetation-dense or building-intensive areas, Gaussian density control relies on local gradient magnitude and lacks semantics-guided priors, resulting in two primary problems:

1) Background Over-Proliferation: Dynamic interferences such as swaying leaves can trigger Gaussian cloning, generating false geometry;

2) Loss of Critical Details: Sub-centimeter structures like tower bolts and insulator steel feet, characterized by low gradient magnitudes, are often misclassified as "low-importance" regions and pruned.

(3) Scenario-Dependent Computational Efficiency

Although the algorithm achieves real-time rendering in open environments, the number of primitives may surge to tens of millions in highly occluded areas (e.g., power line-vegetation overlaps), leading to:

1) Sorting Overhead Surge: The time complexity of radix sort is O(N), and when N>106, single-frame rendering latency may exceed 30 ms;

2) Memory Pressure: Model parameters and intermediate caching for large-scale scenes require several GB of video memory, making deployment on edge devices (e.g., inspection drones) challenging.

These limitations profoundly reveal the core contradictions of 3D Gaussian algorithms in distribution network digital twins: the mismatch between the high-precision modeling requirements for slender structures and the algorithm's anisotropic sensitivity, the lack of semantic awareness under complex background interference, and the scenario-dependent trade-offs between efficiency and generalization capability. Traditional improvement strategies (e.g., post-processing repairs or hardware acceleration) can only partially alleviate these issues but struggle to systematically break through the algorithm's underlying bottlenecks.

To address these challenges, this paper proposes three innovative mechanisms: semantics-guided density control, direction-sensitive covariance optimization, and a lightweight splatting framework.

3. Improved 3D Gaussian Splatting Algorithm

3.1 Semantics-Guided Density Control

To address the issue of foreground blurring caused by Gaussian proliferation in vegetation and building backgrounds, the algorithm constructs a dynamic density control mechanism leveraging pixel-level scene understanding provided by semantic segmentation. First, based on the semantic distinction between power equipment and background elements, differentiated Gaussian proliferation strategies are applied to foreground regions (e.g., power lines, utility poles, insulators) and background areas: in power equipment regions, the cloning and splitting thresholds are reduced to enforce a minimum coverage of three Gaussian primitives per pixel, ensuring complete reconstruction of low-texture targets; whereas in background regions, the splitting threshold is increased to 0.5, combined with periodic pruning operations to remove redundant primitives with opacity below 0.05, thereby suppressing artifact generation. To further enhance background suppression, the algorithm introduces a lightweight adversarial discriminator network that forces the Gaussian distribution in background regions to approximate uniform noise through adversarial training. In this process, the discriminator receives both rendered images and real images, while the generator (i.e., the Gaussian splatting model) minimizes the adversarial loss:

$$\mathsf{L}_{\text{adv}} = \mathsf{E}[\log D(I_{\text{render}})] + \mathsf{E}[\log(1 - D(I_{\text{GT}}))] \qquad (4)$$

This forces the distribution of Gaussian primitives in background regions to avoid generating structural artifacts consistent with the real background. Experimental results demonstrate that this strategy reduces the background noise area ratio to 2%.

3.2 Direction-Sensitive Covariance Optimization

To address the significant geometric variations in power equipment, the algorithm proposes an equipment-adaptive covariance optimization strategy. For power lines, the dominant direction is first extracted from multi-view images (via line segment orientation detection using Hough transform), and a direction-sensitive loss function is designed:

$$\mathsf{L}_{\text{direction}} = \sum \| \mathbf{v}_{\text{Gaussian}} - \mathbf{v}_{\text{dominant}} \|^2 \qquad (5)$$

This forces the principal axis direction $\boldsymbol{v}_{Gaussian}$ of Gaussian primitives to align with the dominant direction $\boldsymbol{v}_{dominant}$ of power lines, avoiding fragmentation issues caused by isotropic optimization. Simultaneously, a continuity constraint is applied to the centers of adjacent Gaussian primitives:

$$\mathsf{L}_{\text{smooth}} = \sum_i \| \mu_{i+1} - \mu_i - d \cdot \mathbf{v}_{\text{dominant}} \|^2 \qquad (6)$$

ensuring uniform distribution of Gaussian centers along the power line trajectory (with interval d = 0.1 m). For rigid structures like utility poles, the algorithm incorporates geometric priors by extracting the principal axis direction of initial Gaussian primitives through Principal Component Analysis (PCA), forcing alignment with the symmetry axis of the pole. An edge alignment loss is introduced:

$$\mathsf{L}_{\text{tower}} = \sum \| \nabla I_{\text{render}} \cdot M_{\text{tower}} - \nabla I_{\text{GT}} \cdot M_{\text{tower}} \|_1 \qquad (7)$$

to ensure sharp reconstruction of corners and edges. For insulator surface details, the algorithm forcibly increases Gaussian density within semantically masked regions (≥5 primitives per pixel) and optimizes surface normals through multi-view photometric consistency constraints, enhancing disc texture and geometric accuracy. In insulator disc areas, a normal consistency loss function is applied:

$$\mathsf{L}_{\text{normal}} = \sum \| \mathbf{n}_{\text{render}} - \mathbf{n}_{\text{multi-view}} \|^2 \qquad (8)$$

where surface normals $\boldsymbol{n}_{multi\text{-}view}$ are derived from multi-view images and aligned with rendered normals $\boldsymbol{n}_{render}$, achieving sub-centimeter accuracy in disc spacing errors.

In the direction-sensitive covariance optimization, the weights of each loss function are systematically tuned through experiments and normalized. The specific allocation is as follows: The direction-sensitive loss function ($L_{direction}$) is used to enforce the alignment of the principal axis of Gaussian primitives with the dominant direction of power lines, playing a decisive role in ensuring the geometric continuity of slender structures. It is assigned a weight of

$(\lambda_1 = 0.40)$. The spatial continuity loss $(L_{continuity})$ constrains the uniform distribution of adjacent Gaussian primitive centers along the power line trajectory, preventing model fragmentation, and is assigned a weight of $(\lambda_2 = 0.25)$. The edge alignment loss (L_{edge}) primarily enhances the sharpness of contours and corners for rigid structures such as utility poles, with a weight of $(\lambda_3 = 0.20)$. The normal consistency loss (L_{normal}) is used to restore insulator disc surface details through multi-view constraints and is assigned a weight of $(\lambda_4 = 0.15)$. The sum of all weights is 1, and the total loss function is expressed as:

$$L_{total} = 0.40L_{direction} + 0.25L_{continuity} + 0.20L_{edge} + 0.15L_{normal} \tag{9}$$

The design of this weight system offers the following significant advantages. First, the normalized weights ensure that each loss term is balanced in terms of numerical magnitude, facilitating stable gradient propagation and avoiding optimization oscillations or convergence difficulties caused by the dominance of any single loss, thereby enhancing the robustness of the training process. Second, the weight allocation intuitively reflects the relative importance of different loss functions in the distribution network 3D reconstruction task: the combined proportion of the direction-sensitive and continuity losses (0.65) highlights the algorithm's prioritized focus on the "continuous reconstruction" of slender structures such as power lines, which is highly consistent with the primary objective of addressing "modeling deficiencies in slender structures" as outlined in this paper. Furthermore, although the sum of weights is fixed, this system retains flexibility for scenario-specific adaptation. For example, in areas with severe vegetation occlusion, (λ_1) and (λ_2) can be appropriately increased to enhance structural robustness, while in insulator-dense regions, (λ_4) can be moderately raised to strengthen surface texture restoration. Finally, the hierarchical allocation of weights reflects the algorithm's multi-scale collaborative modeling philosophy for power equipment, encompassing "macro-direction alignment, meso-contour refinement, and micro-detail recovery." This aligns seamlessly with the overall technical framework of the paper—"semantic-guided density control → direction-sensitive geometric optimization → lightweight progressive rendering"—forming a systematic optimization pipeline. Experimental results demonstrate that this weight configuration effectively coordinates the reconstruction requirements of different power equipment, significantly improving the completeness rates of power lines and utility poles while also ensuring the restoration accuracy of fine components such as insulators. This lays a solid foundation for achieving high-precision and high-fidelity 3D modeling in distribution network digital twins.

3.3 Lightweight Splatting Framework

To balance the high memory demands of full-resolution training with real-time requirements, the algorithm designs a three-stage progressive optimization framework.

First, in the low-resolution stage (1/4 resolution), the coarse-grained representation of the scene is established by rapidly capturing the main structures of power equipment (e.g., utility pole outlines and power line trunks). Subsequently, in the medium-resolution stage (1/2 resolution), covariance matrices and opacity parameters are optimized to refine equipment geometric features and suppress background noise. Finally, in the full-resolution stage (1080p), higher-order spherical harmonic coefficients are employed to enhance textural details (e.g., reflections on insulator ceramic discs and rust patterns on utility poles).

To support large-scale scene processing, a dynamic hierarchical memory management strategy is adopted: nearby Gaussian primitives retain FP32 precision to preserve details, while distant primitives are stored in FP16 format. Combined with an asynchronous loading mechanism, only Gaussians relevant to the current viewpoint are retained in memory. In vegetation-dense areas, distant leaf primitives are stored outside memory in FP16 format and dynamically loaded with precision conversion as the viewpoint approaches. This strategy reduces VRAM usage per scene by 40% while enabling real-time rendering at ≥35 fps under 1080p resolution, meeting the dual requirements of efficiency and precision for distribution network digital twins.

3.4 Algorithm Workflow

The algorithm takes multi-view RGB images (covering all angles of power equipment) as input and achieves end-to-end reconstruction from data to high-precision 3D models through a hierarchical processing pipeline. First, in the preprocessing stage, structure from motion (SfM) and semantic segmentation techniques are combined to extract sparse 3D point clouds from the input images, generating pixel-level equipment masks and background probability maps. The semantic segmentation network accurately distinguishes power lines, utility poles, insulators, and complex backgrounds through multi-scale feature fusion, providing prior knowledge for subsequent optimization.

Based on the preprocessing results, the algorithm performs dense sampling in equipment regions during the initialization stage, injecting multi-scale Gaussian distributions with structural priors (e.g., power line trajectories, tower symmetry): slender ellipsoidal primitives are uniformly distributed along the dominant direction in power line mask regions, while in tower mask regions, Gaussian principal axes are aligned based on principal component analysis (PCA) results to ensure initial geometric rationality.

During the optimization stage, the algorithm refines Gaussian primitives through equipment-adaptive loss functions and adversarial background suppression mechanisms. For power lines, a direction-sensitive loss function constrains the covariance principal axes to align with the extracted dominant direction, while a continuity loss maintains spatial coherence between adjacent primitives. For utility poles, an edge alignment loss enhances sharp reconstruction of corners and contours. For insulators, a multi-view normal consistency loss improves surface detail accuracy. Simultaneously, an adversarial discriminator network dynamically suppresses Gaussian proliferation in background regions, forcing the background distribution in rendered images to approximate realistic noise patterns, thereby separating equipment from interference. This optimization process is executed in parallel on GPUs, significantly reducing resource consumption through dynamic memory management (FP32 for near-field, FP16 for far-field) and an asynchronous loading mechanism.

Finally, in the rendering stage, the algorithm adopts a progressive tile-based loading strategy: visible Gaussian primitives are dynamically scheduled based on the current viewpoint, prioritizing power equipment regions for sub-centimeter detail rendering, while background regions are loaded with lower priority or reduced precision. Through a real-time pipeline of tile-based sorting and blending, the algorithm achieves an interactive frame rate of ≥35 fps at 1080p resolution, supporting real-time user operations such as rotation, zooming, and cross-section observation. This provides a highly responsive visualization platform for planning, inspection, and fault diagnosis in distribution network digital twins.

The algorithm features a streamlined and parallelized design, enabling deployment on edge hardware with moderate computing capabilities. To achieve the described real-time rendering performance, the deployment platform must be equipped with a GPU supporting modern graphics computing instruction sets, no less than 8 GB of dedicated video memory, and sufficient system memory to handle dynamic scheduling of models and data. This configuration ensures that the algorithm maintains high-precision reconstruction and smooth interactive capabilities in complex outdoor scenes, meeting the demands of on-site operation and maintenance for low-latency, highly responsive 3D visualization.

Figure 1 illustrates the flowchart of the improved algorithm proposed in this study.

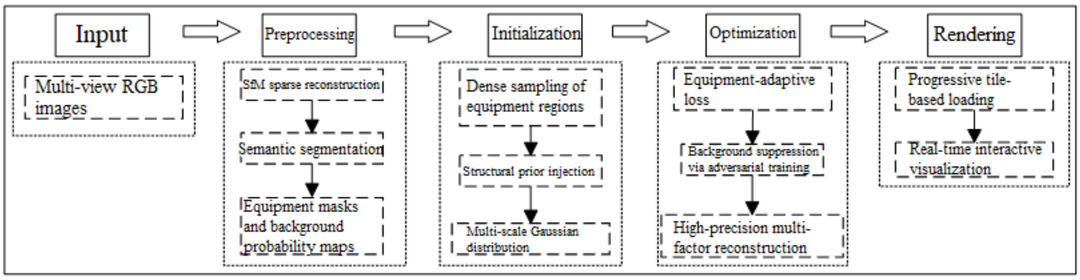

Figure 1. illustrates the flowchart of the improved 3D Gaussian Splatting algorithm proposed in this study.

4. Experiments

4.1 Data Preparation

For this study, a utility pole at a specific location was selected. A drone equipped with a camera was used to capture 64 comprehensive RGB images by circling the pole at 360 degrees, as shown in Figure 2. The images include detailed views of the utility pole and power lines.

Figure 2. Images from Partial Perspectives

4.2 Improved 3D Gaussian Scene Reconstruction

To intuitively demonstrate the improvements of this study on the 3D Gaussian model, each enhancement is incrementally introduced, and the captured distribution network scene is reconstructed. The reconstruction results of the original 3D Gaussian Splatting algorithm are shown in Figure 3.

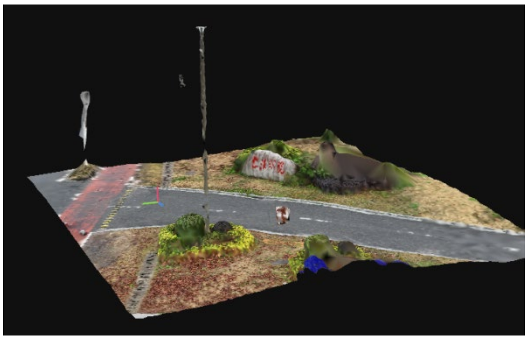

Figure 3. Reconstruction Model Using the Original 3D Gaussian Splatting Algorithm

As seen in Figure 3, the reconstruction performance of the original 3D Gaussian Splatting algorithm is suboptimal: power lines, utility poles, insulators, and other power equipment are incompletely reconstructed, with significant missing elements. Additionally, the environmental background reconstruction is blurred, and background noise is severe. Therefore, improvements to the 3D Gaussian Splatting algorithm are necessary.

First, semantics-guided density control is introduced to reconstruct the 3D scene of the distribution network. This requires classifying objects in the distribution network scene using semantic segmentation algorithms to generate semantic labels. The semantic segmentation is performed on sparse 3D point clouds extracted from the input images. Given the complexity of distribution network scenes, this study employs the NF-PTV2 algorithm—a semantic segmentation method tailored for distribution network point clouds. The semantic segmentation results of the selected scene using the NF-PTV2 model are shown in Figure 4.

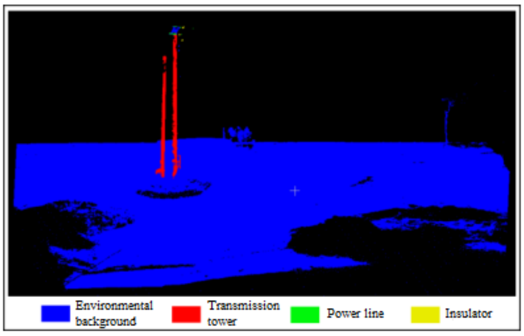

Figure 4. Point Cloud Segmentation Results of the Selected Scene

It is worth noting that the point cloud generated by SfM from images may have partial missing data compared to point clouds directly acquired by LiDAR. However, this will be further addressed and reconstructed in subsequent improvements to restore the original scene more accurately. Semantics-guided density control for reconstructing the distribution network scene involves distinguishing power equipment from complex backgrounds through semantic segmentation. In key areas such as power lines and utility poles, the density of Gaussian primitives is proactively increased to ensure complete reconstruction of low-texture targets. Meanwhile, in background regions, the splitting threshold for primitives is raised, and an adversarial discriminator is introduced to suppress vegetation artifacts. The 3D reconstruction results of the distribution network scene achieved through this improvement are shown in Figure 5.

As seen in Figure 5, compared to the original 3D Gaussian reconstruction results in Figure 3, the introduction of semantics-guided density control significantly enhances the suppression of environmental background artifacts and improves the completeness of power equipment reconstruction. The clarity of the environmental background is notably increased, and the utility pole is fully reconstructed. However, the reconstruction of devices such as power lines and insulators remains suboptimal with the current algorithm. Therefore, direction-sensitive covariance optimization is further introduced to improve the reconstruction accuracy of power equipment.

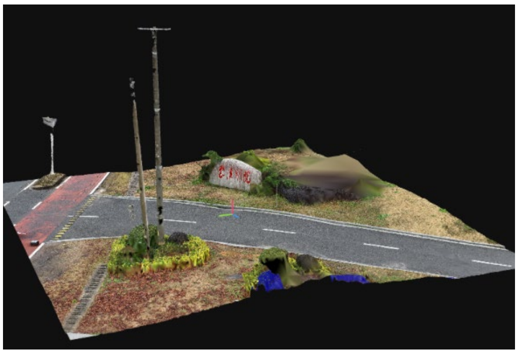

Figure 5. Reconstruction Results After Introducing Semantics-Guided Density Control

Direction-sensitive covariance optimization specifically adapts to the geometric characteristics of power equipment. For slender power lines, a direction-sensitive loss function forces Gaussian primitives to stretch along the dominant direction, combined with continuity constraints to ensure spatial coherence. For utility poles and insulators, geometric priors are utilized to align the principal axes of Gaussians, and an edge alignment loss enhances the sharpness of corners. This improvement effectively addresses the insufficient modeling precision of ultra-slender structures (e.g., power lines) while enhancing the geometric fidelity of rigid equipment. The reconstruction results of the improved 3D Gaussian algorithm after further introducing direction-sensitive covariance optimization are shown in Figure 6.

Figure 6. Reconstruction Results After Further Introducing Direction-Sensitive Covariance Optimization

As shown in Figure 6, after introducing direction-sensitive covariance optimization, the algorithm significantly improves the completeness of power line reconstruction. While Figure 5 barely reconstructed any power line structures, the introduction of direction-sensitive covariance optimization enables a large proportion of power lines to be reconstructed, enhancing the overall completeness of the scene. Additionally, the reconstruction accuracy of utility poles is further improved: in Figure 5, the top structures of the two utility poles were missing, whereas in Figure 6, these structures are substantially refined. Moreover, the insulator structures are successfully reconstructed in Figure 6, with a magnified view shown in Figure 7.

Figure 7. Reconstruction Results of Insulator Surfaces

As seen in Figure 7, insulators on all three lines are reconstructed to a certain extent, and it is clearly visible that the insulator structures are of the tension type.

From the above experiments, it can be concluded that after introducing semantics-guided density control and direction-sensitive covariance optimization to the original 3D Gaussian algorithm, the 3D reconstruction accuracy and completeness of the distribution network scene are significantly improved, as evidenced by comparing Figure 3 and Figure 6. This fully demonstrates the effectiveness of the improvements proposed in this study.

Although the 3D reconstruction results for the distribution network scene are markedly enhanced through these improvements, the time cost for the reconstruction experiments remains high. For the model reconstruction shown in Figure 6, the time consumed is 0.8 hours, indicating a need to further reduce the algorithm's time cost. To address this issue, this study introduces a lightweight splatting framework to the 3D Gaussian algorithm.

The lightweight splatting framework employs a progressive optimization strategy to refine the model in stages: the low-resolution phase rapidly captures the main structures, the medium-resolution phase optimizes covariance and opacity, and the full-resolution phase enhances textural details. This breakthrough overcomes the hardware limitations of large-scale scenes, enabling the algorithm to efficiently handle tens of millions of primitives in vegetation-dense areas, thereby providing feasibility for real-time interaction and dynamic simulation in distribution network digital twins.

Table 1 presents a performance comparison between the final model (after introducing the lightweight splatting framework) and the original 3D Gaussian model, based on the aforementioned improvements.

Table 1. Performance Comparison Between Original and Improved Models

Metric	Original 3D Gaussian	Improved 3D Gaussian
Power Line Completeness Rate	0%	90%
Utility Pole Completeness Rate	50%	95%
Insulator Completeness Rate	0%	80%
Background Artifact Area Ratio	18%	2%
Rendering Frame Rate	≥25 fps	≥35 fps
Reconstruction Time	0.8h	0.4h

As shown in Table 1, the improved 3D Gaussian model demonstrates significant enhancements in reconstruction completeness, clarity, and time efficiency, fully validating the effectiveness of the targeted improvements proposed in this study.

5. Conclusions

This paper addresses three core challenges in 3D reconstruction of distribution networks—insufficient modeling of slender structures, complex background interference, and algorithmic efficiency bottlenecks—by proposing an improved 3D Gaussian Splatting algorithm. First, through a semantics-guided density control strategy coupled with an adversarial discriminator network, the algorithm significantly enhances the completeness and geometric accuracy of key components such as power lines and utility poles while suppressing vegetation artifacts. Next, direction-sensitive covariance optimization and geometry-aware priors are employed to achieve high-precision modeling of power lines and towers, with multi-view normal consistency loss further restoring insulator disc details. Finally, a lightweight progressive splatting framework is introduced, leveraging staged optimization and dynamic memory management to reduce large-scale scene reconstruction time to 0.4 hours while ensuring real-time rendering at ≥35 fps under 1080p resolution, thereby overcoming the traditional trade-off between efficiency and precision.

Experimental results demonstrate that the improved algorithm significantly outperforms existing technologies across multiple metrics, including power line reconstruction completeness, utility pole reconstruction completeness, and background artifact suppression. Specifically, power line reconstruction completeness increased to 90%, utility pole reconstruction completeness reached 95%, insulator reconstruction completeness improved to 80%, and background artifacts were reduced to just 2% in area. Additionally, the rendering frame rate was boosted to 35 fps, while reconstruction time was shortened to 0.4 hours. This achievement further expands the application boundaries of digital twins for distribution networks. The high-precision real-time rendering capability can directly empower augmented reality (AR) systems, enabling three forward-looking scenarios:

(1) AR Inspection and Navigation: Field personnel can use AR glasses to overlay real-time equipment parameters, historical defect markers, and maintenance guidance, enhancing operational efficiency in complex environments.

(2) Fault Simulation and Training: Visualization of fault points (e.g., insulator breakdown locations) and handling procedures in real-world environments, assisting in skill development for new employees.

(3) Remote Expert Collaboration: On-site personnel share AR perspectives, allowing remote experts to annotate equipment hazards in real time and deliver 3D operational guidance, shortening emergency response times.

Future work will focus on integrating the algorithm with edge computing devices to advance distribution network operations toward a "virtual-real fusion and intelligent interaction" model.

Acknowledgements.

This work was supported by the Science and Technology Project of China Southern Power Grid (No. GXKJXM20240054).

References

[1] Wu, Y. Research on Strategies for Digital Transformation of Distribution Network[J]. Automation Application, 2024,65(16):72-74.
[2] Liu, Z.; Pan, F.; Li, F. Intelligent power distribution network digital technology and its application[J]. Lamps & Lighting, 2025,(01):207-209.
[3] Zhao, Z.; Li, X.; Tong, C. Application Practice of Digital Twin Technology in Distribution Network for New Power System[J]. Popular Utilization of Electricity,2023,38(09):59-62.
[4] Sheng, K.; Wu, X.; Li, Z. Application Architecture of New Urban Power System Based on Digital Twin Technology[J].Electric Engineering,2023,(06):100 -103.
[5] Zhang, Y.; Feng, Y.; Lan, Y. Monitoring Method for Operating Status of 10kV Distribution Network Power Equipment Based on Digital Twin Technology[J]. Scientific and Technological Innovation,2022,(36):163-166.
[6] Yu, J.; Zhang, H.; Qi, H.; et al. Application of Digital Twin Technology in Intelligent Operation and Inspection Business of Power Grid[J]. Geospatial Information,2025,23(03):109-113.
[7] Chen, S. Fine modeling of distribution network equipment based on close proximity photogrammetry technology[J]. Mechanical and Electrical Information,2022,(14):84-88.
[8] Xu, J.; Gao, H. Design of Digital Twin Base System for Power Equipment in Distribution System[J]. Electric Power Equipment Management,2024,(18):170- 172.
[9] Wei, S. Research on Insulator Detection and Defect Recogniton of Distribution Network Based on Deep Learning[D]. Guangxi University,2023.
[10] Liu T.; Liu, H. Discussion on Wind Deflection Technology for Large Span Bare Conductors in Distribution Networks[J]. Rural Electrification,2023,(12):1-4.
[11] Li, H. Safety Management of Ground Distance for Distribution Network Lines[J]. Yunnan Electric Power,2004, (05):44-46.
[12] Miao, J.; Xia, Y.; Sun, M.; et al. Application of three-dimensional point cloud processing in the field survey of non-stopping operation of distribution network[J]. China High and New Technology,2025,(02):58-59+91.
[13] Hu, Z.; Yuan, J.; Gong, Y.; et al. Reconstruction of Lead Wires of Power Lines for Live-line Working Robots in Distribution Networks[J]. Control Engineering of China,2021,28(11):2123-2130.
[14] Wang, Z.; Xue, F.; Liu, K. Efficient three-dimensional reconstruction method of SAR image based on neural radiation field[J/OL]. Computer Measurement & Control,1-18.
[15] Wang, J.; Li, Z.; Wang, H.; et al. Highly Robust Multi-view Reconstruction Network for Neural Radiation Field[J]. Geospatial Information,2025,23(04):16-19+ 99.
[16] Shen, Y.; Yang, Q.; Gong, X.; et al. Research on 3D structure reconstruction of power equipment based on multi-feature point fusion[J/OL]. Computer Technology and Development,1-8.
[17] Wang, W.; Tang, B.; Gu, Z.; et al. Overview of Multi-View 3D Reconstruction Techniques in Deep Learning[J]. Computer Engineering and Applications,2025, 61(06):22-35.
[18] Dong, X.; Qu, F.; Zhang, J.; et al. Key design for 3D reconstruction of overhead transmission line corridors based on oblique photography[J]. China High-Tech Enterprises,2016,(18):13-14.
[19] Yu, W.; Lu, J.; Cheng, H. Review of NeRF-based SLAM Research[J]. Computer Systems & Applications,2025, 34(04):18-33.
[20] Wu, Y.; Li, F.; Yu, T.; et al. Power Data Compression and High-precision Reconstruction Based on Residual Dual Attention Mechanism Network[J]. Power System Technology,2022,46(08):3257-3271.